



HAL
open science

Hybridization of Integrated Microwave and Mechanical Power Harvester

Xiaoqiang Gu, Weiqun Liu, Lei Guo, Simon Hemour, Fabien Formosa, Adrien Badel, Ke Wu

► **To cite this version:**

Xiaoqiang Gu, Weiqun Liu, Lei Guo, Simon Hemour, Fabien Formosa, et al.. Hybridization of Integrated Microwave and Mechanical Power Harvester. IEEE Access, 2018, 6, pp.13921 - 13930. 10.1109/access.2018.2814003 . hal-01901541

HAL Id: hal-01901541

<https://hal.science/hal-01901541>

Submitted on 23 Oct 2018

HAL is a multi-disciplinary open access archive for the deposit and dissemination of scientific research documents, whether they are published or not. The documents may come from teaching and research institutions in France or abroad, or from public or private research centers.

L'archive ouverte pluridisciplinaire **HAL**, est destinée au dépôt et à la diffusion de documents scientifiques de niveau recherche, publiés ou non, émanant des établissements d'enseignement et de recherche français ou étrangers, des laboratoires publics ou privés.

Date of publication xxxx 00, 0000, date of current version xxxx 00, 0000.

Digital Object Identifier 10.1109/ACCESS.2017.Doi Number

Hybridization of Integrated Microwave and Mechanical Power Harvester

Xiaoqiang Gu¹, (Student Member, IEEE), Weiqun Liu², Lei Guo¹, Simon Hemour³, (Senior Member, IEEE), Fabien Formosa⁴, Adrien Badel⁴, and Ke Wu¹, (Fellow, IEEE)

¹Poly-GRAMES Research Center, Department of Electrical Engineering, École Polytechnique de Montréal, Montreal, QC H3T 1J4, Canada

²School of Mechanical Engineering, Southwest Jiaotong University, Chengdu, 610031, China

³CNRS and the IMS Research Center, Department of Science and Technology, University of Bordeaux, F-Talence 33 045, France

⁴Laboratory SYMME, Université Savoie Mont Blanc, Annecy le Vieux, 74 944, France

Corresponding author: Xiaoqiang Gu (e-mail: xiaoqiang.gu@polymtl.ca).

ABSTRACT An integrated ambient kinetic and microwave energy scavenger is presented in connection with its strategy of two-level hybridization, namely structural and functional integration of the two dissimilar energy harvesting techniques. Specifically, they are related to two-resonator/transducer integration and simultaneous/collaborative rectification. An F-shaped radiofrequency antenna serves as the microwave energy collector and a Michael Faraday's generator mounted on a mechanical beam cut out of the printed circuit board (PCB) acts as the electrical current producer. Both microwave and mechanical resonators are optimally designed and accommodated on the same substrate with a compact size comparable to that of a credit card (80 mm × 50 mm). The demonstrated hybrid power harvester has a capacity to operate properly with either microwave or mechanical excitation. When both power sources are accessible, it can provide a notable efficiency enhancement compared to the separate harvesting of two single sources. The measurements show that at a typical injecting AC power of -38 dBm, the rectified DC output power could be increased by at least 50 % compared with a direct summation of DC output power through two separate modes. An efficiency enhancement of 85 % can be achieved when diode's injecting power sources are -45 dBm. With a strong resilience, such a hybrid power harvester is able to potentially find its wide practical applications.

INDEX TERMS energy harvester, Schottky diodes, hybrid harvesting, integrated rectifier, mechanical energy, rectenna, wireless sensor networks, internet of things

I. INTRODUCTION

Wireless sensor networks (WSNs) have gained vast interests and become one of the most intensive research fields in the past decade [1, 2]. The WSNs market has the potential to rapidly rise from \$0.45 billion in 2011 to \$1.8 billion by 2024 [3]. As one of the key innovative technologies to realize emerging concepts and applications like smart city or smart transportation, a WSN is defined as an organic connection of geographically scattered tiny devices which operate collaboratively to communicate with each other by wireless links to implement user-defined applications. Obviously, the booming development of WSNs will further redefine and reshape our future life owing to their easy and cheap deployment features [4]. The ever-evolving solid-state technology coupled with the internet of things (IoT) growth has successfully produced sensor nodes with miniaturized size, low cost but high reliability and adequate security [5]. However, one fatal constraint lies in the energy or power

supply side. Conventional wired/battery based technology noticeably cannot provide an ultimate solution.

Due to the constraints of the wired/battery based solution, wireless power harvesting (WPH) has naturally become a main focus of interest recently. Making use of available ambient energy sources, which are usually wasted sources, to power spatially distributed sensor nodes instinctively become the first choice. The WPH systems based on solar energy [6], thermal energy [7], microwave energy [8], and mechanical energy [9] have been reported. Each harvesting technology has undergone fast developments in the past few decades. However, harvesting single power source is sometimes still proved insufficient to power up sophisticated devices because of changing environments. Nowadays, the hybridization of energy harvesters emerges, such as solar-RF [10], thermal-RF [11], mechanical-solar [12], and even thermal-solar-RF [13] power harvesters. As the output of solar and thermal conversion technique is DC power, it could act as a bias of nonlinear devices while rectifying the other

collected power such as mechanical or microwave in a hybrid mode. Though thermoelectric and solar cells are well-developed, they still require a large volume or size to make sure that sufficient energy is converted. In the scope of this work, an integrated harvesting device is proposed to achieve a collaborative mechanical-RF power harvesting mode.

The proposed hybrid harvesting approach can provide a two-stage conversion efficiency enhancement. For the first stage, it is able to harvest more accessible ambient energy sources resulting in more DC output power. Moreover, a collaborative harvesting can shift the operating point of a nonlinear behavior device to another region so to result in a higher global conversion efficiency. The second feature is normally ignored in a hybrid power harvester analysis as it merely adds the multiple outputs, but it does form a second-stage improvement. The two-stage enhancement of conversion efficiency is predicted by theory to provide two times larger the total DC output when compared with single separate energy harvesting modes with the parasitic loss removed. Such a hybrid mechanical and microwave power harvester was first reported in [14], but it appears to be bulky, too fragile, and not suitable for practical applications. That is because it has a separate mechanical unit without an integrated microwave energy collector. In this paper, an integrated hybrid power harvester is demonstrated. A noticeable efficiency enhancement is reported in a low power range (< -30 dBm). A reasonable agreement is obtained between simulated and measured results.

The remainder of this paper is organized as follows. The design details of mechanical and microwave resonators are covered in Section II. Section III explains the principle of collaborative rectification. Separate mechanical and microwave energy harvesting together with collaborative harvesting measurement results and discussion are presented in Section IV. Section V summarizes a comprehensive comparison of up-to-date hybrid energy harvesters. Finally, conclusions are drawn in Section VI.

II. INTEGRATED POWER HARVESTER DESIGN

A. Mechanical Resonator

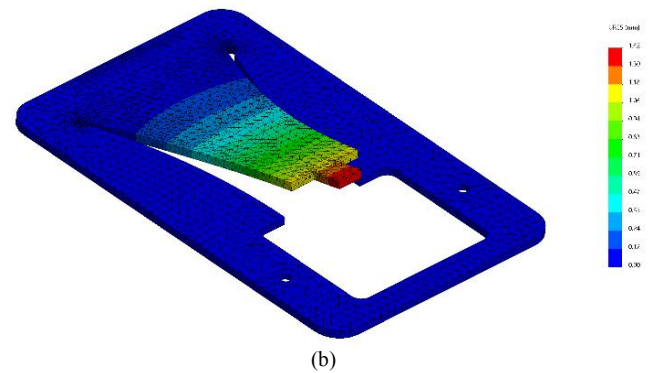
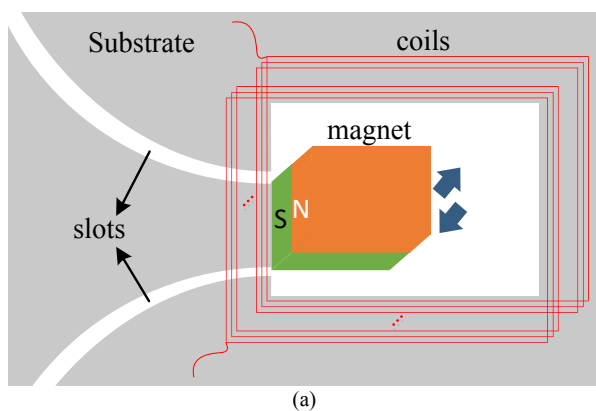


Figure 1. (a) Schematic of mechanical resonator and (b) Finite Element Method (FEM) mechanical simulation of the beam cut out of a dielectric substrate.

The design of a mechanical resonator complies with the pursued full integration goal of the harvester on a substrate with a compact credit-card size (80 mm \times 50 mm). As a result, a low-cost mechanical energy harvester utilizing electromagnetic Faraday effects with a simple topology is adopted in this demonstration. It consists of a permanent magnet which moves relative to coils. In this design, a moving magnet is simpler in terms of implementation as fixed coils will make the electrical connection more reliable. In order to create a mechanical resonator sensitive to the external vibration source, a beam, which acts as a spring, is realized on the same substrate. Two symmetric slots and one rectangular hole are cut off (Fig. 1(a)). The slot follows a circular curve with a proper radius so that the beam width gradually decreases from the fixed end to the free end. This special design is to achieve a more uniform strain distribution in comparison with the rectangular beam design so that it is more reliable and capable of resisting more cracking force. It is especially relevant to the substrate material which has a good electric property for microwave signal but relatively a poor mechanical performance with a small allowable deformation. Besides, the beam design presents easy fabrication requirements in comparison with other shapes, such as spirals, especially for a proper arrangement of the magnet and the coils. An additional advantage is also obtained for integrating the microstrip line-based microwave power harvester in a straightforward manner. The coils are fixed on the board and a permanent magnet is placed at tip of the beam as shown in Fig. 1(a). It is worthwhile to note that the permanent magnet is the mass of the mechanical resonator. When the board is subject to an external excitation, the mechanical resonator (beam and permanent magnet) would oscillate. It creates a relative displacement between the permanent magnet and coils on the board generating electrical energy at the frequency of the mechanical excitation. By carefully choosing the beam width and length, the resonant frequency of the mechanical resonator can be designed at the targeted frequency. With the excitation frequency matching the beam's resonant frequency, the vibration energy harvesting is at its

maximum. The mechanical characteristics of the beam are based on a FEM simulation using SolidWorks as shown in Fig. 1(b). The resonant frequency of the mechanical oscillator is evaluated eventually according to the design requirements. And this resonant frequency is possible to be designed in a range of 30 to 130 Hz. The coil turns are 230 and it forms a rectangular shape in the design with a dimension of 1.7 cm × 1 cm. Key parameters of the mechanical oscillator have been studied in our previous work [15].

B. Microwave Resonator

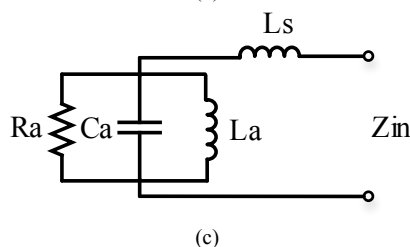
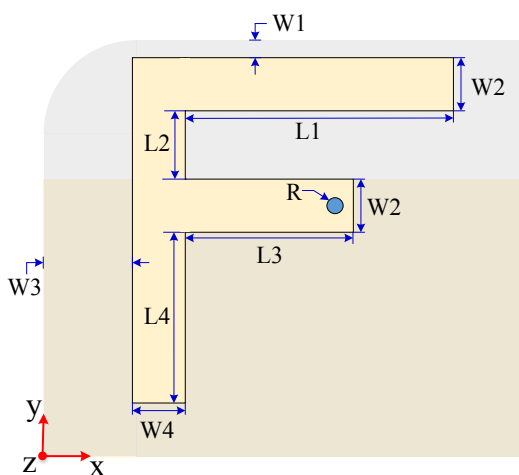
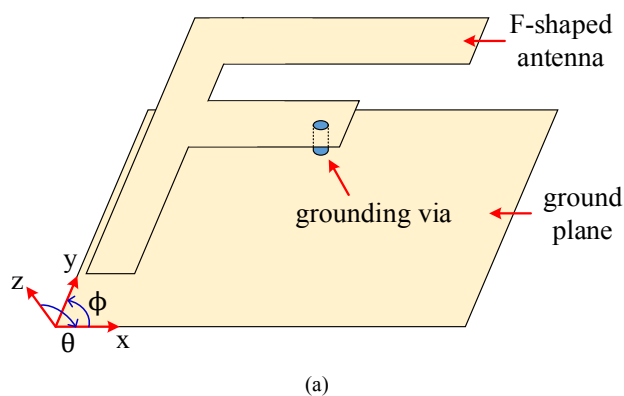


Figure 2. Geometries and an equivalent circuit of the proposed F-shaped antenna: (a) 3-D view with substrate board removed; (b) Top view; (c) The equivalent circuit of the antenna.

In GSM band communication applications, planar inverted-F antenna (PIFA) and inverted-F antenna (IFA) are widely used to overcome the issue of normally a limited space on a

crowded substrate board. The proposed compact F-shaped antenna is the microwave resonator which shares the features of both PIFA and IFA [16]. To realize an omnidirectional radiation, the ground is partly cut off beneath the radiator branch and the edge is aligned along the shorter branch. A 3-D view of the antenna is presented in Fig. 2 (a) with the substrate board removed to clearly show this feature. The geometry parameters defined in Fig. 2 (b) are $W1 = 0.5$, $W2 = 1.5$, $W3 = 5$, $W4 = 1.55$, $L1 = 25.6$, $L2 = 3$, $L3 = 13$, $L4 = 15.6$, $R = 0.4$, in mm.

Antenna design is tedious and inefficient through simulation by a commercial software without a basic understanding of the physical background. Thus, to get a better knowledge of how this antenna behaves, an equivalent parallel RLC resonant circuit is introduced as shown in Fig. 2 (c) [17]. The proposed F-shaped antenna is designed to work at 1.8 GHz. It is printed on the substrate of Rogers RT/duroid 6002 with a dielectric constant $\epsilon_r = 2.94$ and a thickness of 60 mil. The wavelength λ is then calculated by:

$$\lambda = \frac{v}{f} = \frac{1}{f} \sqrt{\frac{\mu_0 \epsilon_0 \epsilon_r}{f}} = \frac{1.75 \times 10^8}{1.8 \times 10^9} = 97.2 \text{ mm} \quad (1)$$

in which f , μ_0 , and ϵ_0 are the operating frequency, the vacuum permeability and permittivity, respectively. The longer branch, acting as the radiator, is a quarter-wavelength transmission line with a length of $L1=25.6$ mm obtained from the full-wave simulation, which is close to the calculated $\lambda/4$ from (1). The capacitance C_a in the equivalent circuit is formed by the radiator and the ground. In order to compensate the capacitance at designated frequency, a shorter branch with a grounding via is introduced in parallel with the longer one, which is supposed to present an inductance L_a . The series inductance L_s is usually caused by the feeding line.

The resonant angular frequency ω_0 can be calculated as:

$$\omega_0^2 = \frac{1}{\sqrt{L_a C_a}} \quad (2)$$

At the resonant frequency, the input impedance Z_{in} is then expressed as:

$$Z_{in} = R_a + j\omega_0 L_s \quad (3)$$

The above analysis can be used to predict the performance of the F-shaped antenna and as a guideline for optimization in the full-wave simulation.

III. COLLABORATIVE RECTIFICATION

As can be seen in Fig. 3, both the mechanical resonator and the F-shaped antenna are collaboratively and harmonically integrated on the same substrate. One RF choke and one DC block are placed between the resonators to prevent any possible interference. Then the combined power goes through a matching network which is used to reduce the mismatch loss between the antenna and diode, and reaches

the nonlinear Schottky diode. The matching network between antenna and rectifier is a traditional microstrip L-Matching network, composing of a series transmission line and a parallel open-circuited stub. Thus, it does not have a large dynamic range in terms of operating frequency and input power. Matching losses are expected at kinetic frequencies since there is no impedance matching network for the kinetic generator in this design. It is actually a very challenging task due to the low-frequency characteristics of the generated electrical signal (as seen in (3), a lumped component with a very high value is indeed necessary to compensate the low frequency of operation). As indicated by the DC current flow presented in Fig. 3, the generated DC current travels to a load resistor through the low-resistive coils. To smooth out AC signals over the load, a large capacitor is connected in parallel with the load resistor. For the packaged Schottky diode, we use a classical Shockley model for the purpose of a theoretical investigation (see Fig. 3). C_p and L_p are packaging capacitance and inductance. C_j and R_j are nonlinear junction capacitance and resistance, respectively. R_s is the series resistance.

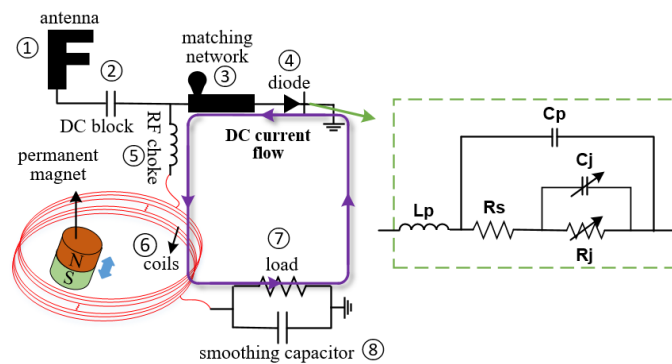


Figure 3. Scheme of the single Schottky diode based collaborative power harvester

According to an early work [18], the rectification process can be broken apart into several parts. The core is the RF-to-DC conversion efficiency which is expressed by:

$$\eta_{RFDC} = \frac{P_{in} \mathfrak{R}_{I0}^2 R_L^2}{R_L + R_s + R_j} \quad (4)$$

where P_{in} is the RF input power. \mathfrak{R}_{I0} is the zero-bias current responsivity and reflects the degree of nonlinearity of any diode. It is defined as the ratio of the short-circuited DC output current by the input power and calculated by $q/2nkT$ for which the variables of q , n , k , and T are electron charge, diode's ideality factor, Boltzmann constant, and operating temperature (Kelvins), respectively. R_L is the load resistor. According to (4), more input power is able to lift up the RF-to-DC conversion efficiency. For example, two identical input powers could double the RF-to-DC conversion efficiency. However, due to the parasitic loss, the total efficiency improvement cannot reach 100%. The parasitic efficiency is defined as the power absorbed by the nonlinear

junction resistance R_j over the total power injecting into the diode as shown:

$$\eta_p = \frac{1}{1 + \frac{R_s + R_j \omega^2 C_j^2 R_s}{R_j}} \quad (5)$$

In Fig. 3, as the nonlinear junction capacitance provides a leaky path for the injecting power, part of power cannot be converted. It can be observed in (5) that the parasitic efficiency becomes larger when a lower-frequency power source is injected. In other words, if a hybrid energy harvesting mode is considered as a combination of separate mechanical and RF energy harvesting, the DC output contribution of the mechanical energy input will be larger. To compare with two separate harvesting modes and show the efficiency improvement of the hybrid harvesting quantitatively, an efficiency gain η_g is proposed here. It is defined as DC output power P_{DC_hy} of the hybrid harvesting over that of a direct superposition of separate RF output power P_{DC_RF} and the mechanical excitation output power P_{DC_me} [15]:

$$\eta_g = \frac{P_{DC_hy}}{P_{DC_RF} + P_{DC_me}} \times 100\% \quad (6)$$

TABLE I
KEY SPICE PARAMETERS OF SMS7630-079LF USED IN ADS SIMULATION

Parameters	Units	SMS7630-079LF
Is	A	5e-6
N		1.05
Rs	Ω	20
Cj0	pF	0.14
Lp	nH	0.7
Cp	pF	0.16

A circuit based on the Skyworks SMS7630-079LF diode has been simulated in Keysight Advanced Design System (ADS) to perform a theoretical analysis. Key SPICE parameters used in the simulation are listed in Table I. The output of mechanical power is modeled as an electrical signal with a typical frequency of 100 Hz. The load resistor is selected as 5.6 k Ω in the simulation. This is close to the optimum loading value at a low-level power reported by our early work [19] which is the same as R_{j0} . Both electrical energy converted from the mechanical power and RF energy are set to be the same and swept from -45 to -30 dBm. The simulated results are presented in Fig. 4. The stacked column is the summation of DC output power from the two separate harvesting modes with values also indicated by the magenta line. The green column is the DC output obtained from the hybrid harvesting mode which is also marked by the dark yellow line.

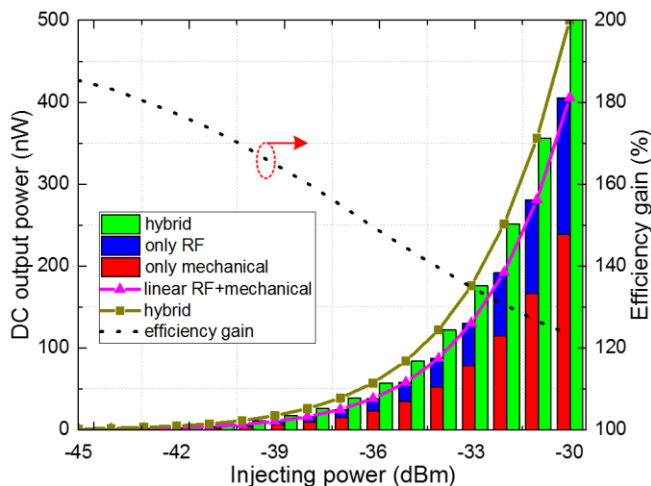


Figure 4. Comparisons of DC output power rectified from hybrid and separate harvesting modes together with efficiency gain performance when both RF and mechanical powers injecting into diode are swept from -45 to -30 dBm.

Firstly, the DC output power from single mechanical energy harvesting mode (red column) is larger than that rectified from RF power only (blue column). It agrees with the aforementioned analysis that a lower parasitic loss of low-frequency energy harvesting is capable of leading to a larger DC output. Secondly, the hybrid harvesting mode provides an enhanced DC output power compared with the summation of DC output power rectified from separate modes. Moreover, the efficiency gain performance is presented in the same figure to clearly show the improvement of a collaborative rectification. The output power is increased by about 85% when both powers are -45 dBm and the improvement drops to about 25% when both are -30 dBm. Schottky diodes with smaller nonlinear junction resistance and capacitance are desired to increase the efficiency gain performance but usually at the expense of a larger matching network loss.

IV. SEPARATE AND COLLABORATIVE MEASUREMENTS, RESULTS AND DISCUSSION

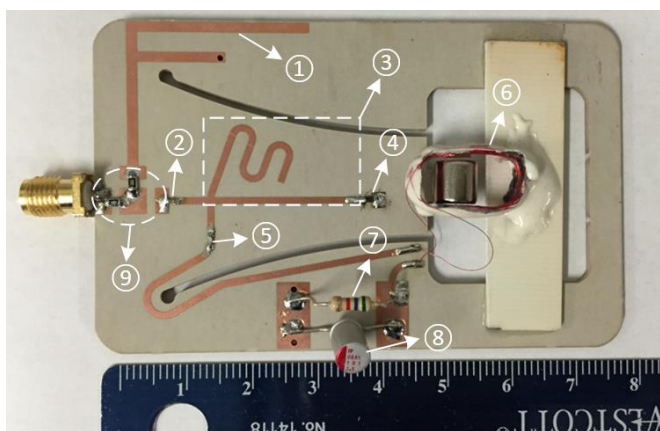


Figure 5. Photo of the experimental prototype of the proposed hybrid microwave and mechanical power harvester.

Figure 5 shows the experimental prototype of the proposed hybrid microwave and mechanical power harvester. The marks of each component match those in the diagram in Fig. 3 except for component No. 9. Indeed, this component was chosen as it enables three types of connection using zero-ohm resistors to complete three different measurements as follows:

- Microwave resonator (antenna) measurement.
- Testing of the rectifying circuit powered by an external signal generator.
- Measurements when F-shaped antenna acting as the microwave energy collector for the rectifying circuit.

A. Measurement and Results of the Mechanical Resonator

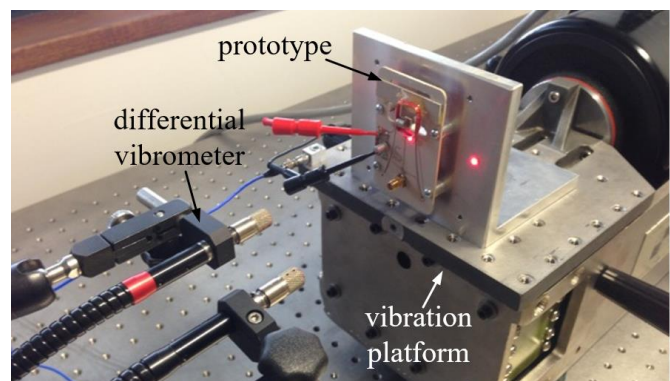


Figure 6. The measurement setup to test the mechanical resonator of the hybrid power harvester.

Figure 6 shows the measurement setup for the mechanical resonator of the proposed hybrid power harvester. The harvester is mounted on a vibration platform. A differential vibrometer allows measuring the relative displacement and the velocity of the beam with respect to the board frame. Fig. 7 shows the experimental root mean square (RMS) open-circuit voltage resulting from the electrical energy generated by the mechanical resonator under different excitations. During the test, the voltage peak shifts to a lower frequency region when the vibration amplitude becomes larger. Specifically, the resonant frequency of the structure is about 88 Hz when acceleration is 5 m/s^2 and decreases to 83 Hz when acceleration increases to 20 m/s^2 . This is a characteristic of the softening mechanical behavior which could be associated with the material behavior. Note that the output voltage saturates at the resonant frequency when acceleration rises to around 30 m/s^2 . Technically, an RMS voltage of 100 mV is the maximum output this integrated mechanical resonator able to offer. During the collaborative measurement, the output voltage is tuned by changing the acceleration (vibration amplitude) while keeping the mechanical resonator at its resonant frequency. As already mentioned, because of the low-frequency nature of the electrical energy, the matching network between the low-resistive mechanical resonator and diode remains a big challenge. For example, in order to obtain -35 dBm of low-frequency power injecting into the diode, RMS output voltage is supposed to be 43.13 mV with the

resonator's internal impedance of 2.3Ω . This means that less than 1% of the generated energy reaches the diode. This could be optimized by increasing the internal impedance of the mechanical resonator. Also, decreasing the impedance of the non-linear device can reduce the mismatch loss as well.

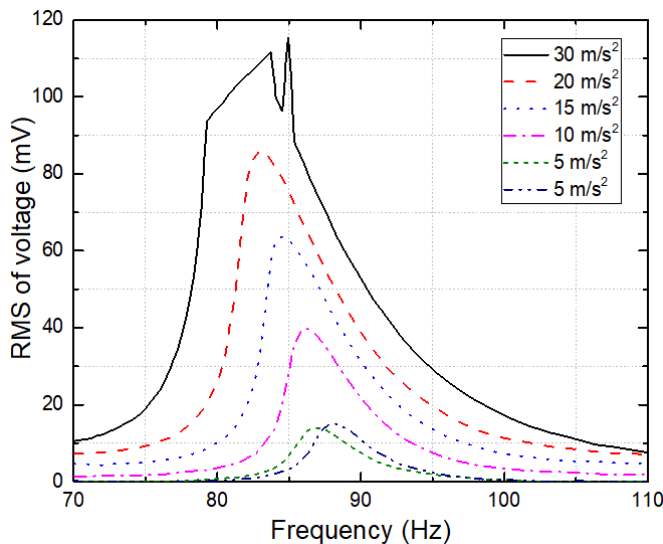


Figure 7. RMS voltage of the electrical energy generated by the mechanical resonator excited by different vibration forces.

B. Measurement and Results of the Microwave Resonator

The input reflection coefficient of the antenna is simulated, measured using an Agilent vector network, and compared in Fig. 8. The measured resonant frequency is slightly shifted from the designated frequency (1.8 GHz). However, the measured reflection coefficient at 1.8 GHz is about -13 dBm and can be considered enough for our application.

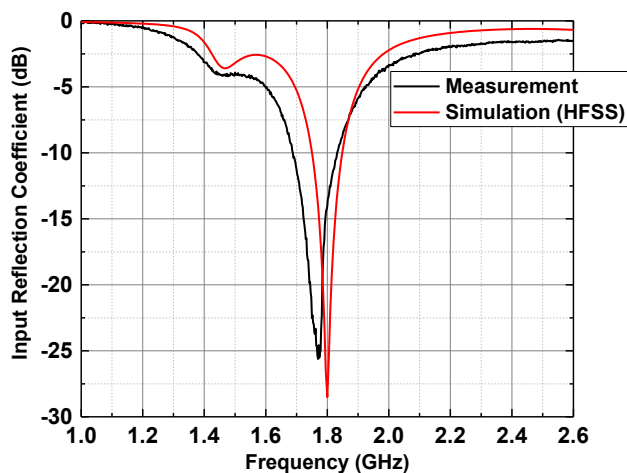


Figure 8. Comparison of simulated and measured input reflection coefficients.

In order to obtain the antenna performance at different receiving angles, the radiation pattern measurement was first completed in a Satimo near-field anechoic chamber which offers an automatic antenna measurement solution in our Poly-

Grames Research Center. The maximum measured antenna gain and efficiency are over 3 dB and around 92 %, respectively. The DC output power depends heavily on the antenna performance. For example, the antenna efficiency is a linear factor embedded in the rectenna global efficiency calculation. The measured results show that the antenna can be a proper candidate for a high-efficient RF energy collector. Assuming a typical illuminating microwave power density P_d of 0.0001 W/m^2 (-40 dBW/m^2) on the antenna, the received power P_r by the antenna can be calculated by [20]:

$$P_r = P_d \cdot \frac{\lambda_0^2}{4\pi} \cdot G \quad (7)$$

in which λ_0 is the vacuum wavelength and G denotes the gain of the proposed antenna. The matching network insertion loss is around 0.24 dB. Based on the above information of the available power density, radiation pattern, and insertion loss of the matching network, the rectified DC output at different receiving angles are plotted in Fig. 9 where the best angle to maximize the receiving power can be extracted.

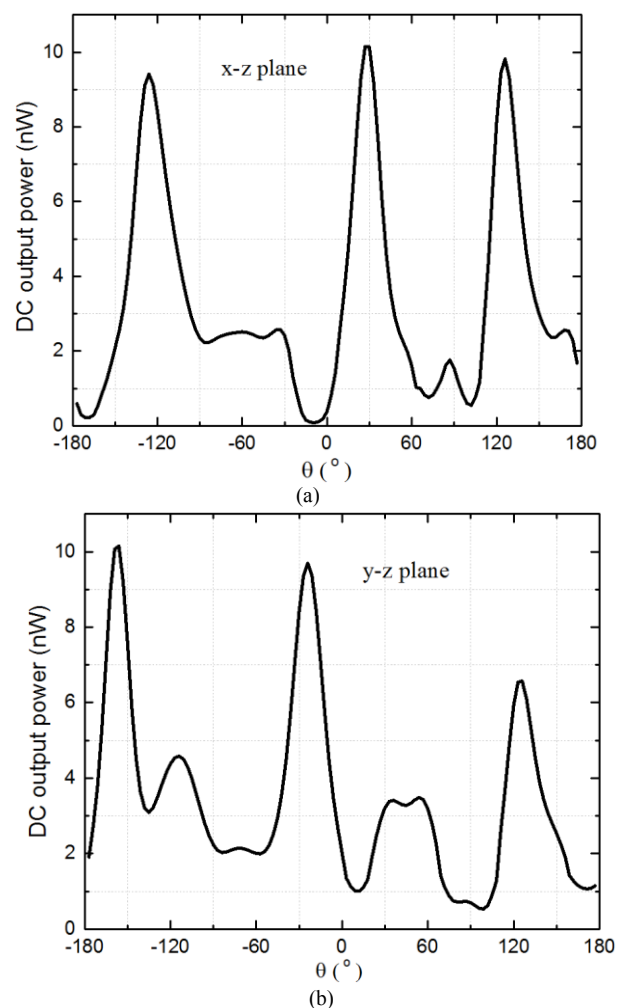


Figure 9. Rectified DC output power by the harvester at different receiving angles when the power density is 0.0001 W/m^2 . (a) x-z plane and (b) y-z plane.

C. Collaborative Measurements and Results

After measuring the mechanical and microwave resonators, a collaborative measurement was conducted in an anechoic chamber as shown in Fig. 10. The main reason to do the measurement in this chamber is to exclude any interference signal in the free space since the GSM band covers the operating frequency of the F-shaped antenna. A stubby antenna connected to a signal generator acts as the RF energy transmitter and is placed about 3 meters away from the receiver side. The collaborative harvester is mounted on a shaker which is driven and controlled by an arbitrary waveform generator as demonstrated in Fig. 10 (b). A miniature accelerometer is attached to the harvester to monitor the vibration acceleration information. The acceleration signal is manipulated by a signal conditioner and finally displayed by an oscilloscope. The AC output signal of the mechanical generator is a sinusoidal wave which has the same waveform as that of the driven force, in accordance with the electromagnetic transduction mechanism. Referring to the readings on an AC voltage meter, the mechanical power provided by the generator can be easily captured. The magnitude and frequency of the driving signal can be tuned to control AC output power from the mechanical generator. A DC voltage meter is used to measure the DC output voltage across the load resistor.

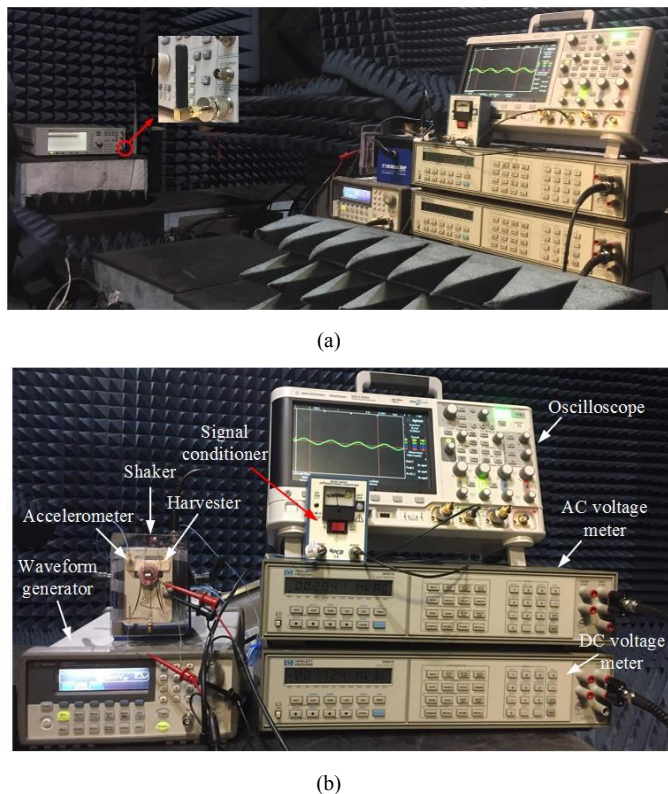


Figure 10. (a) Measurement setup of the hybrid power harvester in our anechoic chamber. (b) Instruments employed for the purpose of monitoring and data recording.

During the collaborative measurement, the microwave and low-frequency electrical powers injecting into the diode were

kept same and swept from -45 to -35 dBm. The integrated harvester was maintained to work at a resonant frequency in order to ensure the maximum vibration energy conversion. The measured results of DC output power are presented in Fig. 11 together with the comparison with the data from ADS simulation. Note that the required acceleration information for the mechanical resonator is listed under each diode's injecting power level. Such vibration levels are possible to obtain in our daily life. For example, the vibration acceleration required to generate the injecting power of -41 dBm is 0.62 g. This can be offered by an operating stand fan at a low speed [21].

Besides the hybrid rectifying mode, separate microwave and mechanical excitation modes were tested individually. Similar to the aforementioned theoretical analysis, in the separate modes, the DC output power rectified from mechanical excitation mode is larger than that from its microwave counterpart. It is clearly observed that the measured DC output from hybrid mode is larger than the linear summation of DC outputs from separate modes, showing a superior performance. The simulated DC output power from the hybrid harvesting mode is also presented for comparison, which shows a good agreement in trend despite little differences. Besides, both measured and simulated efficiency gains are shown with a reasonable agreement. The differences between the measured and simulated data are mainly caused by two reasons. One is the inaccuracy of the SPICE parameters on datasheet used for the theoretical analysis, as they are extracted from massive measurements. A specifically selected diode does not necessarily have the same parameters as on the datasheet. The other is the AC output signal which is not an ideal sinusoidal waveform when a hybrid power harvester operates at a frequency close to its inherent resonant frequency. In the post-process, it is however still assumed to be a sinusoidal wave.

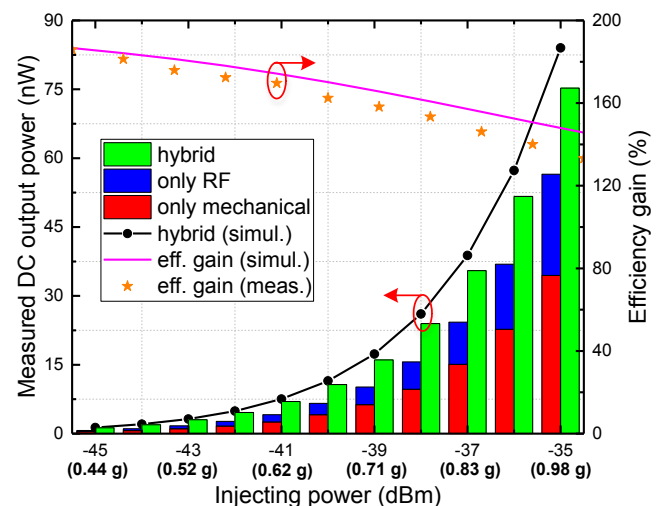


Figure 11. Measured DC output power from separate and hybrid modes together with simulated DC output from the hybrid mode. Comparison of measured and simulated efficiency gain is also demonstrated.

In addition to the considerable efficiency enhancement, such a hybrid power harvester shows a strong resilience in an ever-

changing rectifying environment. Since it is capable of operating individually, it outputs DC power under either microwave or mechanical excitation conditions. However, once the hybrid power harvester is accessible to both power sources, it can provide a noticeably larger DC output, showing a great potential for various practical applications.



Figure 12. Implementation of proposed hybrid energy harvester on a door frame, which takes advantage of the vibration just after the door closes.

Figure 12 shows a typical implementation of the proposed hybrid energy harvester on a door frame. The energy harvester can convert the vibration force into AC power just after the door closes [22]. At the same time, it is free to collect available RF energy in the free space. Although the proposed hybrid energy harvester offers tens or hundreds nanowatt level power when harvesting ambient RF and mechanical energy, it is still able to find possible applications thanks to well-developed CMOS sensor techniques. For example, a dust-size sensor node with only 0.7 nW power computation has been demonstrated in [23]. Our proposed hybrid harvester could be configured to wake up and energize such power-stingy CMOS sensor nodes in further WSNs applications.

V. COMPARISON OF HYBRID ENERGY HARVESTERS

Due to its abundance in urban areas, strong penetration over walls and excellent mobility, RF energy remains one of the most attractive candidates in energy harvesting community. Thus, Fig. 13 compares up-to-date different hybrid energy harvesters all including RF energy harvesting. Hybrid thermal and RF energy harvesting can offer an appreciable efficiency enhancement by using the DC output of thermal energy conversion as a bias of the diode [11]. However, it is worth noting that the reported efficiency enhancement does not count in the loss due to Joule heating on the diode. In other words, from the perspective of global power conversion efficiency, it is more power-efficient for the DC

energy rectified from thermal power to be transmitted to the load directly in an ambient energy harvesting scenario. Moreover, a Thermo-Electric Generator (TEG) is the key component for the energy conversion. Such a hybrid energy harvester usually requires a cooling system or device for a better harvesting performance, leading to relatively higher system complexity.

For hybrid solar and RF energy harvesters, the output of solar cells is also DC power. Theoretically, the global efficiency of hybrid harvesting is degraded similarly to the hybrid thermal and RF energy harvester mentioned above. But hybrid harvesting does help increase diode's RF-to-DC conversion efficiency due to the existence of a DC bias offered by solar energy harvesting [10]. Solar energy harvesting normally has a stronger power density under a good sunlight illumination condition. Meanwhile, limited available operating time of solar cells sets constraints on applications of such hybrid energy harvesters. Outdoor applications rely heavily on sunlight which is variable and dependent on weather conditions. Indoor applications suffer when lights are off at night time.

A hybrid thermal, solar and RF energy harvester is reported in [13]. Theoretically, it can improve the RF-to-DC efficiency dramatically as well. But such an improvement is achieved at the expense of a larger structural size and higher system complexity.

In the scope of this work, mechanical energy intrinsically generates a low-frequency AC signal. It has been combined together with a high-frequency AC signal (RF energy) to produce an efficiency enhancement, particularly in a low power range. Note that neither mechanical nor RF energy is sacrificed to improve the global efficiency. Moreover, the mechanical energy harvesting part could be replaced by a piezoelectric film to shrink the overall size and improve the implementation flexibility [24].

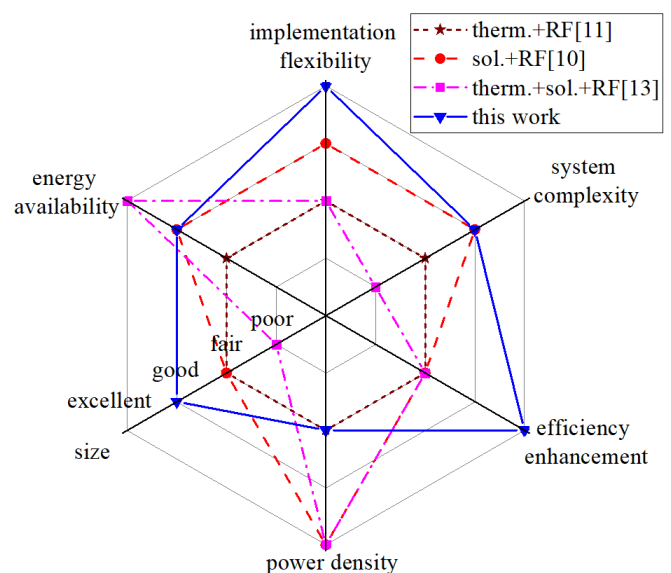


Figure 13. Comparison of different hybrid energy harvesters.

VI. CONCLUSION

This work presents an integrated hybrid microwave and mechanical power harvester. It deploys a compact F-shaped antenna and a traditional electromagnetic generator to realize microwave and mechanical resonators, respectively. Having a size comparable to a credit card, such a hybrid power harvester can offer a typical efficiency performance excited by either microwave or mechanical energy. Once both power sources are available simultaneously, it is able to provide a considerable efficiency improvement. Through comparing with the measured DC output from the hybrid harvesting mode and separate harvesting modes, the efficiency gain reaches 186 % and 153 % when diode's both injecting power sources are -45 dBm and -38 dBm, respectively.

ACKNOWLEDGMENT

The authors would like to express their gratitude to Matteo Andrade-Gazel for his help in the integration design. The authors are also grateful to the technical staff in the Poly-GRAMES Research Center for their outstanding work in fabricating the prototype and measurement support.

REFERENCES

- [1] S. Khan, A.-S. K. Pathan, and N. A. Alrajeh, *Wireless Sensor Networks: Current Status and Future Trends*. France: CRC Press, 2016.
- [2] Z. Sheng, C. Mahapatra, C. Zhu, and V. C. Leung, "Recent advances in industrial wireless sensor networks toward efficient management in IoT," *IEEE Access*, vol. 3, pp. 622-637, 2015.
- [3] P. Harrop and R. Das, "Wireless Sensor Networks (WSN) 2014–2024: Forecasts, Technologies, Players," IDTechEx, Cambridge, United Kingdom, Tech. Rep. 1.1-1.10, 2014. [Online]. Available: <https://www.idtechex.com/research/reports/wireless-sensor-networks-wsn-2014-2024-forecasts-technologies-players-000382.de.asp>
- [4] I. Butun, S. D. Morgera, and R. Sankar, "A Survey of Intrusion Detection Systems in Wireless Sensor Networks," *IEEE Commun. Surveys Tuts.*, vol. 16, no. 1, pp. 266-282, 2014.
- [5] A. A. Babayo, M. H. Anisi, and I. Ali, "A Review on Energy Management Schemes in Energy Harvesting Wireless Sensor Networks," *Renew. Sustain. Energy Rev.*, vol. 76, pp. 1176-1184, Sep. 2017.
- [6] Z. Chen, M.-K. Law, P.-I. Mak, and R. P. Martins, "A Single-chip Solar Energy Harvesting IC Using Integrated Photodiodes for Biomedical Implant Applications," *IEEE Trans. Biomed. Circuits Syst.*, vol. 11, no. 1, pp. 44-53, 2017.
- [7] H. Im *et al.*, "High-efficiency Electrochemical Thermal Energy Harvester Using Carbon Nanotube Aerogel Sheet Electrodes," *Nat. Commun.*, vol. 7, p. 10600, 2016.
- [8] C. H. P. Lorenz *et al.*, "Breaking the Efficiency Barrier for Ambient Microwave Power Harvesting With Heterojunction Backward Tunnel Diodes," *IEEE Trans. Microw. Theory Techn.*, vol. 63, no. 12, pp. 4544-4555, 2015.
- [9] Y. Wu, A. Badel, F. Formosa, W. Liu, and A. Agbossou, "Self-powered Optimized Synchronous Electric Charge Extraction Circuit for Piezoelectric Energy Harvesting," *J. Intell. Mater. Syst. Struct.*, vol. 25, no. 17, pp. 2165-2176, 2014.
- [10] K. Niotaki, F. Giuppi, A. Georgiadis, and A. Collado, "Solar/EM Energy Harvester for Autonomous Operation of a Monitoring Sensor Platform," *Wireless Power Transfer*, vol. 1, no. 1, pp. 44-50, 2014.
- [11] M. Virili *et al.*, "Performance Improvement of Rectifiers for WPT Exploiting Thermal Energy Harvesting," *Wireless Power Transfer*, vol. 2, no. 1, pp. 22-31, 2015.
- [12] C. Xu and Z. L. Wang, "Compact Hybrid Cell Based on a Convulsed Nanowire Structure for Harvesting Solar and Mechanical Energy," *Adv. Mater.*, vol. 23, no. 7, pp. 873-877, 2011.
- [13] M. Virili *et al.*, "EH Performance of an Hybrid Energy Harvester for Autonomous Nodes," in *Proc. IEEE Topical Conf. Wireless Sensors and Sensor Netw.*, Jan. 2016, pp. 71-74.
- [14] C. H. Lorenz, S. Hemour, W. Liu, A. Badel, F. Formosa, and K. Wu, "Hybrid Power Harvesting for Increased Power Conversion Efficiency," *IEEE Microw. Wireless Compon. Lett.*, vol. 25, no. 10, pp. 687-689, 2015.
- [15] X. Gu, S. Hemour, and K. Wu, "Integrated Cooperative Radiofrequency (RF) and Kinetic Energy Harvester," in *Proc. IEEE Wireless Power Transf. Conf.*, Taipei, Taiwan, May 2017, pp. 1-3.
- [16] A. Rennings, M. Rauf, P. Waldow, and I. Wolff, "A Compact Single/dual-band Printed Inverted-F Type Antenna Structure," *ACES*, New York, Apr. 2004.
- [17] R. Bancroft, *Microstrip and Printed Antenna Design*. Atlanta, GA: Noble, 2004.
- [18] S. Hemour *et al.*, "Towards Low-power High-efficiency RF and Microwave Energy Harvesting," *IEEE Trans. Microw. Theory Techn.*, vol. 62, no. 4, pp. 965-976, 2014.
- [19] C. H. P. Lorenz, S. Hemour, and K. Wu, "Physical Mechanism and Theoretical Foundation of Ambient RF Power Harvesting Using Zero-bias Diodes," *IEEE Trans. Microw. Theory Techn.*, vol. 64, no. 7, pp. 2146-2158, 2016.
- [20] C. A. Balanis, *Antenna Theory: Analysis and Design*, 3rd ed., New York: Wiley, 2005.
- [21] M. F. B. Ab Rahman and S. L. Kok, "Investigation of useful ambient vibration sources for the application of energy harvesting," in *Proc. IEEE Student Conf. Res. Develop.*, 2011, pp. 391-396.
- [22] S. Roundy, P. K. Wright, and J. Rabaey, "A study of low level vibrations as a power source for wireless sensor nodes," *Comp. Commun.*, vol. 26, no. 11, pp. 1131-1144, Jul. 2003.
- [23] T. Shimamura *et al.*, "Nano-watt power management and vibration sensing on a dust-size batteryless sensor node for ambient intelligence applications," in *IEEE Int. Solid-State Circuit Conf. Dig. Tech. Papers*, 2010, pp. 504-505.
- [24] X. Gu, S. Hemour, and K. Wu, "Cooperative Radiofrequency (RF) and Piezoelectric Energy Harvesting for Global Efficiency Enhancement." in *Proc. 32nd URSI GASS*, Aug. 2017, pp. 1-1.